Year One Report: "Advanced Modeling and Test Methods for Radiation Effects on Microelectronic Devices"

Dr. Robert A. Reed and Dr. Robert A. Weller

Electrical Engineering and Computer Science Department
Institute for Space and Defense Electronics
2014 Broadway, Suite 200
Nashville, TN 37203 USA

Tel (615) 343-2702 / FAX (615) 343-9550
email: robert.reed@vanderbilt.edu
robert.a.weller@vanderbilt.edu

NASA Goddard Contact:

Ken Label
NASA Goddard Space Flight Center
Code 562, Greenbelt, MD 20771
Phone: (301) 286-2153

4/30/2007

"Advanced Modeling and Test Methods for Radiation Effects on Microelectronic Devices"

Co-Investigators:
Dr. Robert Reed and Dr. Robert Weller
Vanderbilt University
Electrical Engineering and Computer Engineering Department

I. Abstract/summary:

The safety of human and robotic missions depends critically upon the reliability of electronic systems. Space radiation effects are among the greatest environmental threats to the safety of manned and robotic missions. Take, for example, life support electronics. While the crew on a manned mission may be well protected from radiation hazards, the critical life support electronics may be near the skin of the craft and relatively unprotected. Radiation effects in electronics range from loss of data to catastrophic failure. In advanced electronics, effects caused by the passage of a single energetic particle through a sensitive device are the most serious problem; while many different electrical effects have been observed, these phenomena are collectively described as single-event effects (SEEs).

Radiation effects data from newer devices, including such essential components as Focal Plane Arrays and state-of-the art digital/mixed signal electronics, have demonstrated that existing models have significant errors. For example, using CREME96 for optocouplers underestimates single event rates, overestimating survivability. Standard models also produce inaccurate estimates for single event rates in SiGe, CMOS technologies and low-dose-rate degradation of bipolar linear ICs.

The safety and reliability of forthcoming long-duration missions will depend critically on using the most advanced electronics available and providing radiation/fault-tolerant system design. Advances in microelectronic technologies have created a situation in which time-tested methodologies for radiation-hard electronic design, validation, and verification can no longer assure the safety of electronic parts and systems used for space exploration. Therefore, a new tool is needed so that the reliability and safety of space systems can be assessed. This tool must be based upon first-principles physics computations so that engineers can predict accurately the radiation tolerance of emerging technologies in the space environment.

The report provides advances in the development new technology modeling approaches for radiation induced Single Event Transients (SETs) in Focal Plane Arrays and advance CMOS devices and Single Event Upsets (SEUs) in Silicon Germanium (SiGe) Heterojunction Bipolar Transistors (HBTs) and advanced CMOS devices.

II. Background

NASA and DOD spaceflight missions often rely on system level solutions to mitigate the impact of a single microelectronic component failure due to exposure to the space radiation environment. This has proven to be a very effective and useful approach. These techniques range from the use of error correction techniques for data memory to redundant subsystems. In some drastic cases, system engineers have opted to power down subsystems during times when the radiation environment is severe—preventing data collection or posing significant risk to the subsystem. An example of the latter is the NICMOS instrument on the Hubble Space Telescope; radiation events in a microelectronic device require instrument operation to be discontinued while passing through the South Atlantic Anomaly region of the earth trapped radiation environment. A detailed understanding of the reliability/survivability of microelectronic devices when exposed to the space radiation environment is critical for sound system engineering decisions.

The success of a system engineering approach to radiation-effects analysis depends on the following factors: 1) A conservative model of the radiation environment for evaluating the extent to which radiation threats may compromise mission goals. 2) Measurements of component responses to terrestrial radiation sources for bounding on-orbit device performance. 3) A comprehensive physical model to predict the

energy deposited in the semiconductor by terrestrial and space radiation sources. 4) Physics-based component response models to predict and analyze electrical performance degradation.

The success of such analysis depends critically on the models used for the interaction and transport of radiation through spacecraft structures and semiconductor materials. These models serve as a bridge between ground-based laboratory data and prediction of on-orbit radiation performance. They also provide guidance as to the test methods and laboratory measurements needed for such predictions.

Advances in microelectronic technologies and economic pressure to use commercial electronic parts have created a new situation in which time-tested methodologies for radiation-hard electronic design, validation, and verification can no longer assure the safety (as defined in NFS 1852.223-70) of electronic parts and systems used for space exploration. In particular, several recent developments[2] suggest that it may be appropriate to revisit the methods and models used in predicting on-orbit radiation response of modern electronics and advanced sensors. Recent radiation effects experiments on these modern technologies show trends inconsistent with current models: 1) SiGe HBTs, 2) large scale photodetectors, 3) SOI/SOS CMOS, 4) IR Focal Plane Arrays (FPAs), 5) CCDs, and 6) advanced CMOS. In particular the existing models have the following shortcomings:

- Exclude combined effects from direct and indirect ionization by incident particles
- Do not account for the angular dependence of the recoiling nuclei produced by proton-induced spallation reactions or elastic collisions
- Exclude the charge collection by diffusion
- Have limited capability to analyze detailed geometrical effects, i.e., edge effects, isolation trenches, buried oxides
- Have no method for modeling effects associated with the complex spatial variation of charge deposited by individual ion strikes.

The simple truth is that the existing techniques, developed circa 1980, fail to provide accurate reliability/survivability estimates for most modern technologies. Mature technologies have been scaled to dimensions where new phenomena challenge some of the basic simplifying assumptions of radiation effects models, which were developed for technologies fabricated in the late 70's early 80's. Some recent results suggest that current methods could yield predictions that overestimate or underestimate on-orbit error rates by an order of magnitude or more.

The next sections provide a description of our research to improvement modeling radiation effects for various technologies.

III. RADSAFE Validation (Vanderbilt University, NASA/GSFC, BAE, APL, SNL)

Introduction

Single Event Effects (SEE) analysis techniques akin to the rectangular parallelepiped (RPP) model [1] have been shown to provide accurate reliability/survivability estimates for Single Event Upsets (SEU) in certain technologies, while for other technologies and effects the model has been shown to be inadequate. Specifically, the applicability of Linear Energy Transfer (LET) as an engineering metric has been questioned for many years [2, 3, 4 and references within]. Until recently, careful analysis of experiments has shown that, for the most part, these concerns could be resolved by modifying the RPP model.

Fig. 1 displays SEU data taken on a modern high-reliability, radiation-hardened SRAM (described in [3]). The data were taken at three different facilities, for a range of ion energies, and all ions were normally incident (we will look more closely at these data in the experimental section). The key point, for now, is the lack of correlation between the measured cross section and ion LET; in particular, notice the large discontinuity in the data. These data are difficult to use to predict reliable on-orbit SEU rates using techniques based on an LET distribution defined by a simple RPP geometry. In [4], Dodd *et al.* presented data showing a poor correlation of effective cross section with effective LET for a hardened SNL SRAM.

Our simulation tool called MRED (Monte Carlo Radiative Energy Deposition, a Geant4 based tool for

predicting energy deposition in small volumes) was used in [2, 3] to show that SEU cross section could depend on ion energy and species, rather than just LET, when nuclear reactions dominate the response. In [3] we used our simulation tool to show that the low LET data in Fig. 1 (collected at TAMU) was due to nuclear reactions. However, these studies lacked experimental data over a range of ion energies and species.

In this research, we provide experimental evidence and extended simulation results to confirm that LET can not be used to provide a well behaved description of the SEU response for this SRAM and that all physical processes must be included in order to predict the response. Furthermore, we discuss the impact of certain systematic errors for Geant4 based simulations. Finally, we predict the on-orbit event rate using MRED and compare this to the observed rate on a NASA mission to Mercury. MRED predictions, which include all relevant physical process for radiation transport, are shown to be in close agreement with the average observed SEU rate on a NASA mission to Mercury. The traditional Integral RPP (IRPP) method, which does not include the contribution from ion-ion reactions, falls well below the observed rate.

Experimental Results

New SEU cross section data were collected on two radiation hardened SRAMs (called SRAM#1 and SRAM#2) at two SEE test facilities: Lawrence Berkeley National Laboratory (LNBL), and the National Superconducting Cyclotron Laboratory (NSCL). The ions used are listed in Table 1. The ion energy and associated LET are also listed in Table 1. Fig. 1 compares these data to the data given in [3]. (The details of the test setup are identical to those described in [3]). The legend provides the cyclotron-tuned energy, not the ion energy on the target. Error bars representing one standard deviation (68% confidence interval) are included; the symbols hide the error bars for the cases where they cannot be seen.

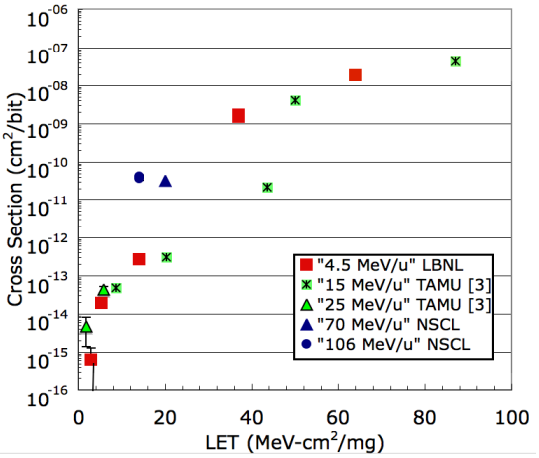


Fig. 1: Measured SEU cross section versus LET for normally-incident ions at several different facilities. The data show two orders of magnitude difference at a fixed

The intent of this testing was to study the dependence of the measured SEU cross section on incident ion energy and species for normally incident ions. As stated in the introduction, the discontinuities at several values of LET clearly show that direct ionization from the primary particle (or LET) cannot be used to describe the trends in the data. For example, comparing the measured cross section for ions that have a LET of 14 MeV·cm^2/mg, we see that the cross section using the 14.4 GeV Xe ions at NSCL (blue circle) is two orders of magnitude higher than that measured with the 180 MeV Ar ions at LBNL (red square). The high atomic mass (***A***), high energy ion produces a higher SEU cross section than the low ***A***, low energy ion. The same can be said for ions with LETs of 20 MeV·cm^2/mg (9.25 GeV Xe ions and the 729 MeV Cu ions). However, comparing data near an LET of 40 MeV-cm^2/mg shows that using the low ***A***, low energy ion produced a higher SEU cross section than that with the high ***A***, high energy ion. There appears to be no simple predictable trend with ion LET (even ionization track radius), species, and/or ion energy!

TABLE I
Ions used for testing SRAM#1

Test Facility	Species-Atomic Mass	Energy (MeV)	LET (MeV-cm²/mg)	Computation Method
LBNL	N-15	68	2.9	Full
LBNL	Ne-20	90	5.3	Full
LBNL	Ar-40	180	14	Full
LBNL	Kr-86	387	37	Full
LBNL	Xe-136	612	64	No Nuclear Reactions
TAMU	Ne-22*	523	1.8	Full
TAMU	Ar-40*	494	8.7	Full
TAMU	Ar-40*	919	5.8	Full
TAMU	Ag-109*	1200	44	No Nuclear Reactions
TAMU	Au-197*	2000	87	No Nuclear Reactions
TAMU	Cu-63*	729	20	Full
TAMU	Ag-109*	665	50	No Nuclear Reactions
NSCL	Xe-136	14416	14	None
NSCL	Xe-136	9520	20	None

* From [2]

In Section III, we show that one needs to include all physical interaction processes in order to explain these data. We are able to do this using a Geant4 based simulation tool, MRED, that includes high fidelity

physics models for all physical processes.

Finally, we note that at high LET values, where the cross section is near 4×10^{-8} cm^2, direct ionization dominates the response. At these LET values, the LBNL and TAMU results agree and are consistent with the expected sensitive volume geometry as measured by laser testing and as determined via TCAD [3]. We also note that [5] provides data that show that the dosimetry at NSCL is consistent with other radiation effects test facilities. It is most certainly true that these facilities use sufficient dosimetry techniques such that the data represent reality and are not an artifact induced by facility differences.

Discussion of Ground Testing

LET is defined as the mean energy lost by an ion per unit path length in collisions with electrons of the material and is a good quantity to characterize the energy available to produce ionization (free charge). Ionization from the primary particle is called direct ionization. Indirect ionization, induced by secondary particles from ion-ion reactions, can result in large amounts of energy deposited near SEE sensitive structures.

In general, measured SEE cross sections will include a contribution from three interaction processes between the ion and the target semiconductor: 1) direct ionization induced by the primary ions, 2) indirect ionization via Coulombic scattering between target atoms and the incident ion, and 3) indirect ionization from nuclear reactions between the incident ion and the target nucleus. The relative contribution depends on the number of sensitive volumes, cell critical charge, amount and location of high-Z materials, and the ion species, energy, and fluence used in the testing [2, 3].

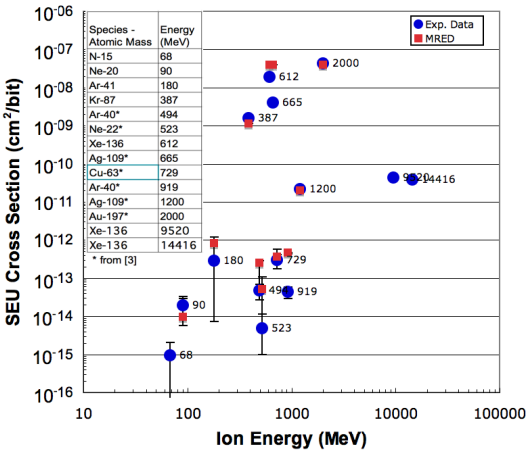


Fig.2 Comparison of ground test results to MRED predictions.

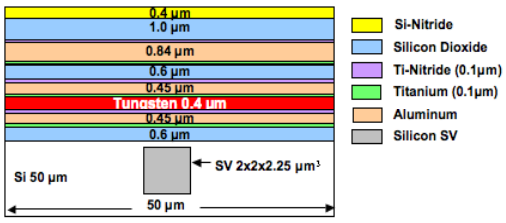


Fig. 3. Sensitive volume and overlayer used for MRED simulation

The MRED simulation tool was used to simulate the 12 lowest energy ions listed in Table I. Current limitations within Geant4 prevent the simulation of nuclear reactions for ions with a large atomic mass [2]. We chose not to do simulations for the two ions used at NSCL. Fig. 2 shows the measured SEU cross section (data from Fig. 1) for each ion (blue circles). The measured data contain error bars that represent a 95% confidence interval. The figure also shows a least squares fit to the cross section data obtained from MRED simulations. The error bars on the simulation results represent the estimated error in the prediction due to systematic errors in Geant4 (see the Appendix). The abscissa is the total ion energy. The inset in the figure lists the ion energies. Each data point is also labeled by the ion energy. MRED simulations are in good agreement with measured data.

MRED fully simulates each of the processes defined above for an ensemble of incident primary particles, applies the appropriate interaction cross sections, and records the energy loss of the primary particle and all secondary particles within a defined box (called the sensitive volume). In [3] we determine the sensitive volume geometry for this SRAM#1 to be $2\times2\times2.25$ µm^3. The surrounding material is consistent with the overlayers used to fabricate the SRAM (Fig. 3).

The cross section for depositing a specific energy, E, or greater can be computed from MRED results by defining a critical charge (equivalently a critical energy) with which the SEU cross section can be estimated.

Simulation results can be separated into two categories, SEU induced by direct ionization and those induced by indirect ionization. Each of these categories must be analyzed separately. Geant4 is much more accurate at predicting effects from direct ionization than for indirect ionization (see the Appendix). We determined that the simulation results are dominated by direct ionization effects for Ar(387 MeV), Kr(665 MeV), Xe(612 MeV), Au(2 GeV), and Ag(1.2 GeV) ions. Indirect ionization effects dominate for all other ions.

The experimental data presented in Fig. 2 were used to determine the best value for critical charge by finding the least squares best fit. The value for the critical charge for direct ionization events was determined to be 1.02 pC (or 23 MeV), while for indirect ionization the best fit to the data resulted in a range from 0.71 pC (or 16 MeV). This is not a surprising result given that there are known systematic errors in Geant4 (see the Appendix) that cause an underestimation of the SEU cross section. Notice that the 0.71 pC is 30% less than 1.02 pC, or energy deposition is under predicted by about 30%, which is consistent with the conclusion of the Appendix.

SEE On-Orbit Rates and Predictions

A Monte Carlo simulation program, such as MRED, may be viewed as a machine for determining a probability distribution by repetitive sampling. It is particularly useful when direct analytical computation of the distribution is difficult or impossible. MRED can be configured to compute the energy deposited by a large number of ions with randomly chosen initial trajectories, produce a histogram of the resulting values, normalize the histogram to unit area, and scale by the width of the histogram bins to obtain a discrete approximation to a continuous probability density. In [2] we provide a discussion of the technique used to predict the single event upset rate using MRED. We have updated the method described in [2] by allowing an ion selection biasing based on the ion's relative abundance.

MRED was used to compute the SEU event rate, $\boldsymbol{R}(E_d)$, for depositing energy in the sensitive volume for the solar-quiet/solar minimum galactic cosmic ray (GCR) background. The environment was predicted using the models on the CREME96 website [7]. A computed event rate of 8.1×10^{-9} errors/bit/day was found by evaluating $\boldsymbol{R}(E_{crit} = 16$ MeV).

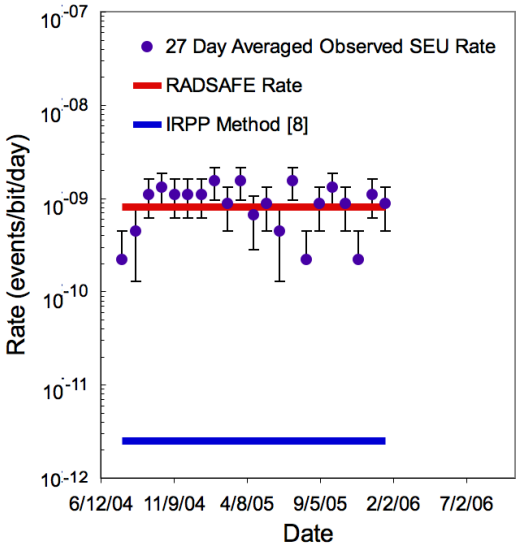


Fig. 4. Comparison of the MRED based event rate predictions for SRAM#1 to measured data on a NASA mission to Mercury. Also plotted is the predict rate using IRPP [8]. We assumed 100 mils of Al shielding.

One of NASA's missions to Mercury utilizes 40 SRAM#1s. Fig. 4 gives a plot of the observed 27 day averaged rate for SEUs (error bars for the blue symbols are one standard deviation). This figure also shows the prediction from MRED (labeled RADSAFE) and the Integral RPP method [8]. The measured 27 day averaged SEU on-orbit rate is between 2.2×10^{-10} and 1.5×10^{-9} errors/bit/day. The MRED prediction of the SEU rate is in agreement with the average observed rate. Using the classical approach for rate predictions, a rate of 2.5×10^{-12} errors/bit/day was estimated [8]. It is a factor of 88 to 618 lower than the rate observed on the spacecraft. The MRED rate is in much better agreement with the observed rate than that predicted by the classical method. The reason behind this is that MRED includes all relevant physical process for radiation transport while the traditional IRPP method does not include the contribution from ion-ion reactions.

Conclusions

Ground based SEU experiments on a radiation hardened SRAM confirm the contribution of heavy ion-induced nuclear reactions to the measured SEU cross section. The same SRAM was observed to have an on-orbit rate that is underestimated by IRPP event rate predictions. MRED simulations that include all of the necessary physics correctly estimate the SEU response of the SRAM for both the space and the ground based radiation environments. The failure of LET to accurately predict observed SEUs for a hardened SRAM will have a dramatic impact on other single event effects. One of the most important is Single Event Latchup (SEL).

Appendix

One of the critical issues in the understanding of SEUs is the correct determination of the energy deposited by the fragmentation of heavy nuclei as a result of nuclear reactions. These reactions are particularly important in two regimes. The first regime is operation in a low LET ion background. The other regime is ion reactions in which nuclei react with target species.

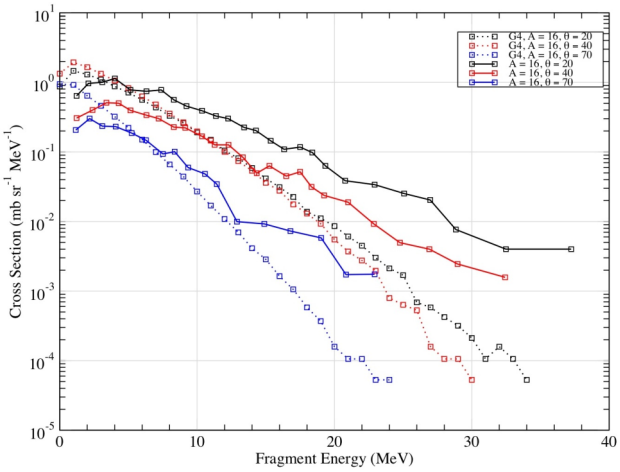


Fig. 5: Comparison of Geant4 and experimental results from [9] for 180 MeV protons on aluminum. Geant4 dramatically underestimates the energy.

The underlying physics in each of these regimes is quite different, and not very well characterized. Triple-differential cross sections, measured by fragment energy, fragment mass, and fragment angle, are the minimal requirement to understand how these reactions deposit energy in semiconductors. Unfortunately, it appears that only one experiment has produced data of the quality needed for use in simulations. Kwiatkowski [9] carried out this experiment, using 173 MeV protons on an aluminum target. Fig. 5 compares experimental results for oxygen residual nuclei to the nuclear fragmentation models currently available through Geant4. Dashed lines connect Geant4 results and solid lines connect the experimental data.

Current breakup models predict heavy fragment production with significantly lower energy than was observed in this experiment. Comparison to the Kwiatkowski results shows that, for protons on aluminum, the scale energy is 30-40% too low. This results in an under-production of more than an order of magnitude of the most energetic fragments, which results in under-prediction of the energy deposited, SEU cross sections, and SEU event rates.

References

[1] E. L. Petersen, "Predictions and observations of SEU rates in space," *IEEE Trans. Nucl. Sci.*, vol. 44, no. 6, pp. 2174-2187, 1997.

[2] R. A. Reed, R. A. Weller, R. D. Schrimpf, M. H. Mendenhall, K. M. Warren, and L. W. Massengill, "Implications of nuclear reactions for single event effects test methods and analysis," *IEEE Trans. Nucl. Sci.*, vol. 53, no. 6, pp. 3356-3362, 2006.

[3] K. M. Warren, R.A. Weller, M.H. Mendenhall, R.A. Reed, D.R. Ball,; C.L. Howe, B.D. Olson, M.L. Alles, L.W. Massengill, R.D. Schrimpf, N.F. Haddad, S.E. Doyle, D. McMorrow, J.S. Melinger and W.T. Lotshaw, "The contribution of nuclear reactions to heavy ion single event upset cross section measurements in a high-density SEU hardened SRAM," *IEEE Trans. Nucl. Sci.*, vol. 52, no. 6, pp. 2125-2131, 2005.

[4] P. E. Dodd, J. R. Schwank, M. R. Shaneyfelt, V. Ferlet-Cavrois, P. Paillet, J. Baggio, G. L. Hash, J. A. Felix, K. Hirose, and H. Saito , "Heavy ion energy effects in CMOS SRAMs," paper A-1, *presented at the conference for RADECS*, Athens, Greece, 27-29 September 2006.

[5] R. Ladbury, R. A. Reed, P. W. Marshall, K. A. LaBel, R. Anantaraman, R. Fox, D. P. Sanderson, A. Stolz, J. Yurkon, A. F. Zeller, and J. W. Stetson , "Performance of the high-energy single-event effects test Facility (SEETF) at Michigan State university's national Superconducting Cyclotron laboratory (NSCL)," *IEEE Trans. Nucl. Sci.*, vol. 51, no. 6, pp. 3664-3668, 2004.

[6] T. Koi, "Ion transport simulation using GEANT4 hadronic physics," *presented at the Monte Carlo 2005 Topical Meeting*, Chattanooga, Tennessee, USA, 17-21 April 2005.

[7] Available on the web at http://creme96.nrl.navy.mil/.

[8] Nadim Haddad, private communications.

[9] K. Kwiatkowski, S. H. Zhou, T. E. Ward, and V. E. Viola,, "Energy deposition in intermediate-energy nucleon-nucleus collisions," *Phys. Rev. Lett.*, vol. 50, no. 21, pp. 1648-1651, 1983.

VI. Focal Plane Arrays (Vanderbilt University, NASA/GSFC, AFRL)

Introduction

Hybrid focal plane arrays (FPA) are increasingly being used in space applications because of their flexibility in infrared applications, reliability, low cost, high-density resolution, and on-chip signal processing [1]. FPAs are often used on satellites planned for long orbits in harsh proton environments requiring exceptional reliably when exposed to radiation, and hybrid visible array technology is especially important due to advantages over CCD-based imagers in high proton exposure applications. A better understanding of how radiation-induced energy is deposited in these devices will help lead to better prediction techniques and a greater understanding of experimental results. Accurate modeling tools will help designers better predict the on-orbit response of these increasingly popular devices.

Previous Monte Carlo prediction models for these devices have shown inconsistencies with experimental data [2]. In this research we demonstrate a high-fidelity rate-prediction approach, based on Monte Carlo simulation and a mathematical model that accounts for multiple events that affect a single pixel during the integration time. We also show that using a single-value LET and path length calculation underpredicts the differential experimental spectra.

Experimental Description

Hybrid focal plane arrays consist of a readout integrated circuit (ROIC) and detector array fabricated separately and then joined together with interconnects such as indium columns [3]. The focal plane arrays in this study are visible FPAs consisting of a silicon P-i-N 128 × 128 detector array with a hardened complementary metal–oxide–semiconductor (CMOS) ROIC [4]. The pixel pitch is 60 μm. Proton radiation studies were performed at the Crocker Nuclear Laboratory (CNL) of the University of California, Davis (UC Davis). Full radiometric characterizations were performed at each radiation dose level to determine the impact of the radiation on dark current, noise, responsivity, sensitivity, and dynamic range both pre and post radiation [4]. The total ionizing dose response of this array has been described in [4]. This research focuses on the proton transient data acquired at low fluxes generating sparse hits to the array

The devices were irradiated with low flux levels to obtain sparse hit rates with 63 MeV protons at an angle of 45°. The silicon P-i-N detectors were biased to 15V resulting in full depletion, and exposures were carried out at 277 K.

Modeling Focal Plane Array

The Monte Carlo code used in this study is MRED (Monte Carlo Radiative Energy Deposition), a GEANT4 based tool [5]-[9]. The structure used to simulate the FPA can be seen in Figure 1. Sensitive region corresponds to the region in which energy deposition must occur to produce a transient event. The top and bottom of the sensitive volume are flush with the top and bottom of the surrounding material which is also silicon. Simulations using MRED included all physics processes that are relevant for radiation effects applications, including electromagnetic and hadronic processes, and elementary particles that live long enough to be tracked. Simulated protons are incident at an angle of 45 degrees with energy of 63 MeV.

The effects of the finite integration time were simulated in a manner analogous to the computation of pile up in an ordinary nuclear spectrum. Each event in the Monte Carlo simulation represents one, and only one, primary particle. For finite integration times, there is a small but non-negligible probability of multiple hits on a single pixel (pile up). Post-processing of simulations included the addition of Gaussian noise observed in the experimental data and pile up to account for the small fraction of multiple hits.

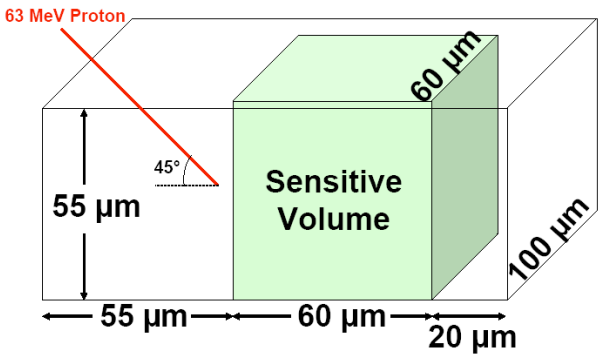


Figure 1. Structures used to represent one pixel of silicon p-i-n detector array. The entire structure is made of silicon and the shaded regions are sensitive to the proton irradiation.

Results and Discussion

The inclusion of all physical radiation transport processes in the simulation, accounting for pile up, and the inclusion of the measured random noise spectrum provide an accurate description of the experimental data for this device with no adjustable parameters. Figure 2 shows a differential spectrum of the counts per fluence as a function of the number of electrons deposited in the sensitive volume, comparing the experimental data with the simulation results. Conversion to units of electrons from the simulated energy deposited in the sensitive volume was accomplished by dividing the deposited energy by 3.6 eV per electron, and the conversion gain of the experimental data was extracted from the device parameters characterized during device testing. The agreement between the two curves is excellent to around 85×10^3 electrons. Past this region there is significant statistical error in the experimental data. Most points represent one, or at most two, counts in that channel, and most bins are zero counts. The observable Gaussian spectrum at low electron counts is due to the expected non-radiation-induced noise in the pixel array.

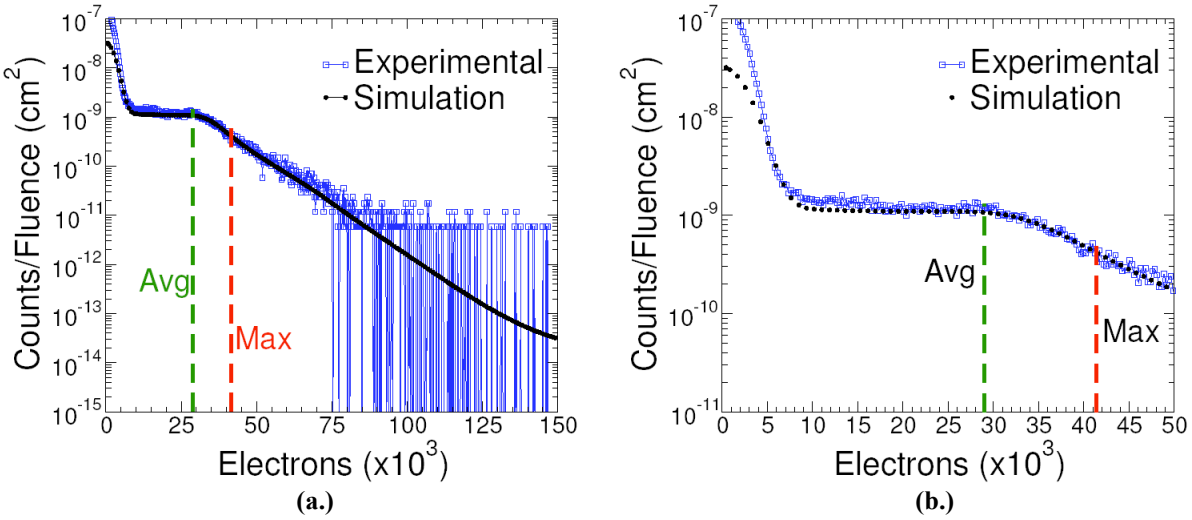


Figure 2. Differential spectrum of counts per unit fluence for 63 MeV protons incident on the silicon detector structure from figure 1 for (a.) the entire spectrum, and (b.) a subset. The computed and measured total cross sections agree closely with each other and approximate the geometric cross section.

The dashed lines in Figure 2 represent the expected average and maximum number of electrons deposited in the structure from a constant-LET and path length distribution calculation. The dashed line labeled "Avg" is the electron counts resulting from an average path length through the structure, and the dashed line labeled "Max" is the electron counts from a maximum path length. With a constant LET of 1.92 keV/µm, and a maximum path length of 77.78 µm, the maximum number of electrons that can be

created in the structure is 41,400. The constant LET method predicts that no events will deposit more electrons than this. Therefore, a constant LET does not predict the occurrence of the large energy depositions and, more subsequently, it does not describe the shape of the curve above 41,400 electrons.

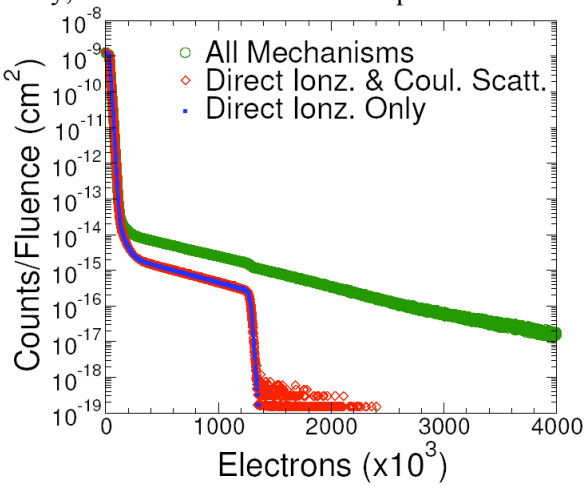


Figure 3 Single particle MRED simulations (no pile up) comparing reaction mechanisms. The large open circles represent the simulation of all physical processes, the open diamonds include direct ionization and Coulomb scattering, and the small filled squares include only direct ionization.

The simulations shown in Figure 2 include primary direct ionization, Coulombic and nuclear contributions, and the portions of the curve visible are largely the result of direct ionization. The constant LET approximation considers only direct ionization, but a path length analysis can only address averages while even primary ionization has fluctuations. The contribution of nuclear reactions is not large until beyond approximately 115,000 electrons, as seen in Figure 3. Here we compare reaction mechanisms for a simulation including a single particle (no pile up). It isn't until approximately 1,350,000 electrons that the Coulomb scattering contributions become noticeable.

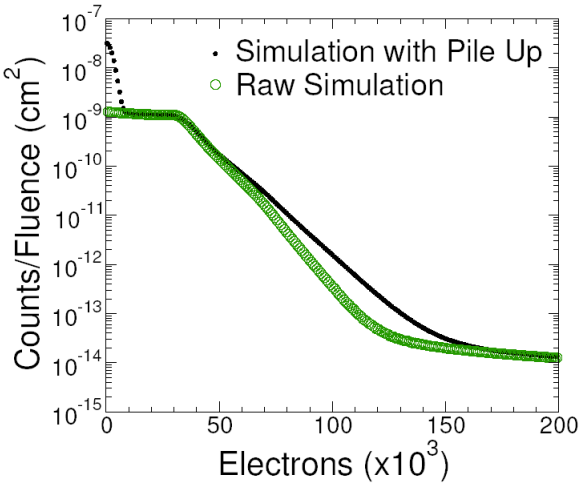


Figure 4 MRED simulation before and after the noise Gaussian and pile up are applied.

Figure 4 compares the MRED simulations before and after the effects of pile up were included in post-processing of the data. The shape of the sloped region between 50 and 200 × 10^3 electrons is affected by the finite number of pixels that receive multiple hits during one integration period. The correction applied is a very general transformation of an arbitrary single-particle spectrum for the case in which the average number of hits per pixel is μ. The transformation inherently includes multiple hits of all orders,

and can be used without numerical difficulty from very low fluxes well into the photon-counting region, where tens or hundreds of particles can hit a pixel in a single integration period. For the data in Figure 2, μ =0.08. The effect of this transformation is shown in Figure 4. A Gaussian noise distribution most noticeable in low electron region was also added to the simulation in post processing to describe system noise. The width of the Gaussian was determined by the experimental data. No adjustable parameters were used.

Conclusion

In this research we show for the first time that when sufficiently complete physics is brought to bear, the results of proton irradiation of an imager can be predicted in greater detail than the resolution of the experiment reveals. Moreover, the effects of individual mechanisms on spectral shape can be separated and studied individually. The imager is an archetype for any silicon device, and the ability to comprehensively model radiation interactions with it is an important milestone in the goal of a priori prediction of device response via Monte Carlo methods in an arbitrary radiation environment.

References

[1] D. A. Scribner, M. R. Kruer, and J. M. Killiany, “Infrared focal plane array technology,” in *Proc. IEEE*, vol. 79, pp. 66-85, Jan. 1991.

[2] S. Onoda, T. Hirao, J. S. Laird, T. Wakasa, T. Yamakawa, T. Okamoto, Y. Koizumi, and T. Kamiya, “Development of Monte Carlo modeling for proton induced charge in Si pin photodiode,” *IEEE Trans. Nucl. Sci.*, vol. 51, pp. 2770-2775, Oct. 2004.

[3] J. C. Pickel, “Novel devices and sensors,” 1993 IEEE Nuclear and Space Radiation Effects Conference Short Course, Snowbird, UT, July 1993.

[4] J. E. Hubbs, M. E. Gramer, D. C. Arrington, G. A. Dole, D. Maestas-Jepson, S. E. Takeall, “Total Ionizing Dose and Proton Radiation Characterization of Si P-i-N Visible Hybrid Focal Plane Arrays,” *Proc. of SPIE,* vol. 5902, pp.

[5] C. L. Howe, R. A. Weller, R. A. Reed, M. H. Mendenhall, R. D. Schrimpf, K. M. Warren, D. R. Ball, L. W. Massengill, K. A. LaBel, J. W. Howard, Jr., and N. F. Haddad, "Role of Heavy-Ion Nuclear Reactions in Determining On-Orbit Single Event Error Rates," *IEEE Trans. Nucl. Sci.*, vol. 52, no. 6, pp. 2182-2188, Dec. 2005.

[6] K. M. Warren, R. A. Weller, M. H. Mendenhall, R. A. Reed, D. R. Ball, C. L. Howe, B. D. Olson, M. L. Alles, L. W. Massengil, R. D. Schrimpf, N. F. Haddad, S. E. Doyle, D. McMorrow, J. S. Melinger, and W. T. Lotshawand, “The contribution of nuclear reactions to single event upset cross section measurements in a high-density SEU-hardened SRAM technology,” *IEEE Trans. Nucl. Sci.*, vol. 52, no. 6, pp. 2125-2131, Dec. 2005.

[7] A. S. Kobayashi, D. R. Ball, K. M. Warren, R. A. Reed, N. F. Haddad, M. H. Mendenhall, R. D. Schrimpf, and R. A. Weller, “The effect of metallization layers on single event susceptibility,” *IEEE Trans. Nucl. Sci.*, vol. 52, no. 6, pp. 2189-2193, Dec. 2005.

[8] S. Agostinelli et al., “Geant4-a simulation toolkit,” *Nucl. Instrum*. *Method Phys. Res. A*, vol. 506, pp. 250-303, 2003.

[9] M. H. Mendenhall and R. A. Weller, “An algorithum for computing screened coulomb scattering in geant4,” *Nucl. Instrum. Phys. Res. B*, vol. 227, pp. 420-430, 2005.

V. SEUs in SiGe HBTs (Vanderbilt University, NASA/GSFC, Georgia Tech, Auburn)

Introduction

This work presents a new Galactic Cosmic Radiation (GCR) event rate calculation for the IBM 5AM Silicon-Germanium Heterojunction Bipolar Transistor (SiGe HBT) based on fundamental physical processes. A multiple sensitive volume model for this technology was developed based on experimental and simulation results obtained over the last five years [1-5]. The event rate calculation was performed for two different circuit designs: a baseline master-slave D flip-flip (M/S DFF) shift register and a Radiation-Hardened-by-Design (RHBD) variant of the M/S DFF employing dual-interleaving of two unhardened stages to provided limited decoupling of the storage cells; both of these designs are outlined in [3] and the references therein. Each register design consisted of 127 stages, which were operated from 50 Mbps to approximately 6 Gbps during Single Event Upset (SEU) testing.

The GCR event rate for the RHBD M/S DFF shift register design is a factor of 3.5 less than the baseline M/S DFF design. The event rate for both of these designs is dominated by direct ionization events, since the threshold Linear Energy Transfer (LET) for both designs is less than 5 MeV·cm^2/mg [3]. Vulnerability to direct ionization means that the flip-flops can experience soft errors due to ionization produced by just the primary particle; ionization resulting from secondary spallation fragments is a second order effect at best. The broadbeam data for these designs from [3] is shown in Fig. 1. These suggest that the GCR event rate for the RHBD design should be much less than the baseline design, since the cross section is substantially lower for increasing angle, which favors the space environment because most particles in the space environment are incident at large angles. In fact, 50% of GCR is incident at angles greater than 60° based on simple solid angle calculations using a cone.

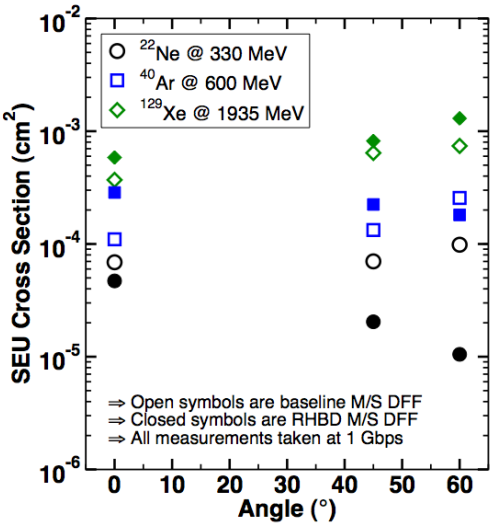


Fig. 1: Broadbeam experimental data for both the baseline and RHBD M/S DFF shift registers, adapted from [3].

SiGe HBTs have a unique response to ionizing particles incident at off-normal angles, characterized by a substantial reduction in the SEU cross section [1-3]. However, previous experimental data sets [2] have shown that at large angles (i.e., ≥ 60°) the cross section of these devices begins to approach what was measured at normal incidence – recovering part of the initial cross section decrease. Since 50% of GCR is incident at angles greater than 60°, this may account for the small difference in GCR event rates for the two shift register designs.

Energy Response Model Development

The GCR event rate calculation for both shift register designs was based on and validated via the experimental data [3] shown in Fig. 1 and detailed 3D Technology Computer-Aided Design (TCAD) simulations [4, 5]. The cross section of the RHBD device decreases with increasing angles of incidence, particularly for neon, though the cross section of the unhardened design does not. Any model developed for use in an event rate calculation must be able to reproduce both of these trends, something that has plagued SiGe HBT event rate calculations.

The multiple sensitive volume model developed for the IBM 5AM SiGe HBT is shown in Fig. 2. These volumes were designed based on the Ion Beam Induced Charge Collection (IBICC) data in [4] and the TCAD simulations in [4, 5]. The concept of using multiple sensitive volumes simultaneously is relatively new [6, 7]; this work relies on the methods of [7]. Utilizing multiple sensitive volumes stems from the need to model progressively more complex charge transport effects as a result of device geometry and process engineering. The lightly doped substrate of most SiGe HBTs and the presence of Deep Trench Isolation (DTI) require the use of multiple sensitive volumes. Multiple sensitive volumes have enabled accurate rate calculations for SiGe HBTs, which was not previously possible.

The broadbeam data and TCAD simulations alluded to a sensitive volume structure that was some hybrid combination of thick and thin Rectangular Parallelepiped (RPP) volumes. The real challenge in designing static energy deposition volumes for SiGe HBTs is matching the charge collection mechanisms at normal incidence and at larger angles. Due to the incident ion's interaction with the DTI at large angles, the charge collection efficiency

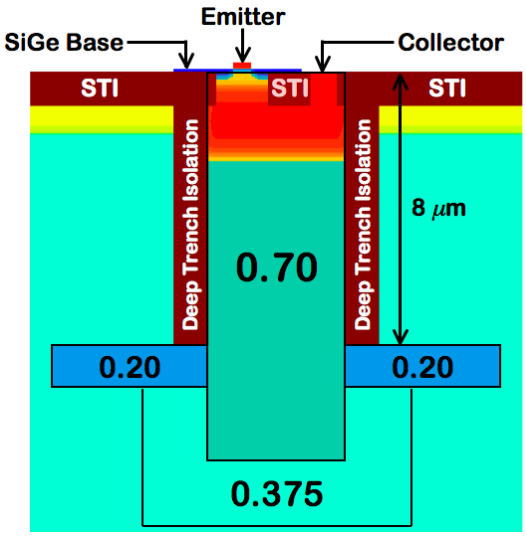


Fig. 2: 2D rendering of the composite, weighted multiple sensitive volume model for the IBM 5AM SiGe HBT. The weights of the volumes are labeled.

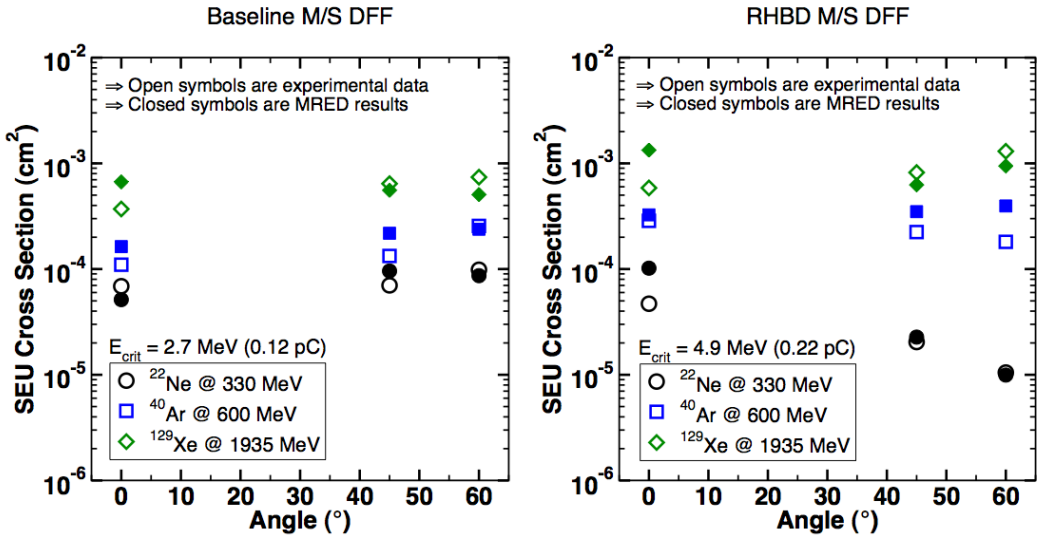
drops due to the lack of electrostatic potential modification in the substrate [5]. However, at normal incidence the charge collection depth can exceed 10 μm [4]. The sensitive volume ensemble shown in Fig. 2 is designed to reproduce these effects.

The sensitive volumes do not operate autonomously, simply returning the amount of energy deposited within their individual boundaries. They function as a whole by forming the components of a "master" sensitive volume whose total deposited energy is represented by the linear combination of the energy deposited within the smaller volumes. As shown in Fig. 2, each volume in the summation has a weighting coefficient. This approach to modeling complex sensitive regions is described in [7].

To verify that the sensitive volume model would accurately reproduce the broadbeam data shown in Fig. 1, Monte Carlo Radiative Energy Deposition (MRED) [8] was used to duplicate the broadbeam experiments for the three ions and three angles reported in [3]: ^{22}Ne, ^{40}Ar, and ^{129}Xe at 0°, 45°, and 60°. The results of the simulations are shown in Figs. 3(a) and 3(b). It is clear from the simulation data points that the MRED multiple sensitive volume model is able to reproduce the experimental results with reasonable fidelity. It is important to note that the *same* model yields experimentally consistent results for *both* shift register designs by the appropriate choice of critical energy (E_{crit}). This is facilitated by the combination of thin and thick RPP volumes used simultaneously to accurately predict the device response.

Critical energy (E_{crit}) is the required amount of energy that must be deposited in a sensitive volume, or in this case a linear combination of several sensitive volumes, to induce a SEU. As stated earlier, the total deposited energy is calculated as the linear sum of energy depositions within individual sub-volumes. E_{crit} is analogous to Q_{crit}, differing only by the constant factor of 22.5 MeV/pC.

The data reproduction displayed in Fig. 3 was achieved by fitting the MRED energy deposition cross section using E_{crit} as the independent variable. The nine data points, one for each ion and angle combination, were then scaled by 127 to match the number of shift register stages since only a single transistor was simulated and the shift registers are made of many transistors. The data were then scaled by an additional constant factor of 3 (baseline M/S DFF) or 6 (RHBD M/S DFF). The additional *ad hoc* scaling factor is meant to account for the average number of sensitive transistors per stage at a particular data rate – 1 Gbps in this case. The TCAD modeling in [5], and the analysis here, indicate that the E_{crit} of the RHBD M/S DFF is nearly 2*x* greater than the E_{crit} of the baseline M/S



Figs. 3(a) and 3(b): MRED reproduction of the experimental data shown in Fig. 1 using the multiple sensitive volume structure shown in Fig. 2. 3(a) shows the MRED simulations compared to experimental data for the baseline M/S DFF and 3(b) shows the same for the RHBD M/S DFF – some data points are coincident. Note that critical energies have been derived from this analysis.

DFF. Since the RHBD design almost doubles the number of transistors in the DFF, 14 versus 26, the number of transistors attached to the sensitive nodes also doubles, which is the source of the 3*x* and 6*x* scaling factors. This same phenomenon is also observed in the E_{crit} for the two circuit designs.

Fitting of the simulation SEU cross section results to the broadbeam data yields an E_{crit} for both of the shift register designs, which can then be used to derive a calibrated event rate based on additional MRED virtual irradiation experiments. Furthermore, the E_{crit} values derived from these MRED simulations, 2.7 MeV and 4.9 MeV, agree to within 21% and 8.5% respectively based on the values reported in [5], which were calculated via 3D TCAD. This independent means of confirmation lends credence to the method employed here.

Event Rate Calculation

The event rate was calculated for the GCR environment as defined by CREME96 [9] under "Solar Quiet" "Cosmic-Ray Maximum" conditions. The event rate computations were performed using MRED as described in [8]. MRED was used to virtually irradiate the 3D TCAD structure over 4π sr with approximately 1×10^9 ions distributed according to their relative abundance across all the ions that CREME96 provides between $1 \le Z \le 92$.

As shown in Fig. 4, the GCR event rate for each of the shift registers was calculated as the intersection of the proper E_{crit} with the event rate curve. The baseline M/S DFF shift register has a calculated GCR event rate of 1.3×10^{-5} events/day/sensitive device and the RHBD M/S DFF shift register has a GCR event rate 3.5*x* lower at 3.7×10^{-6} events/day/sensitive device.

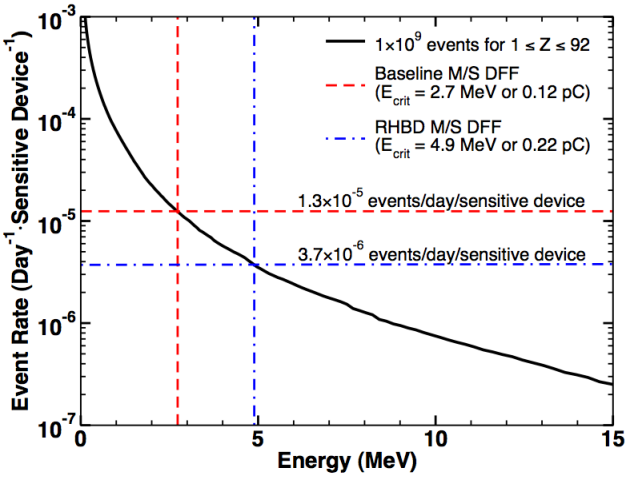


Fig. 4: GCR event rate calculations for the baseline and RHBD M/S DFF shift registers. The critical energies used to derive the event rates were calculated via the analysis discussed in regards to Fig. 3

The event rate calorimetry was performed using the same TCAD structure employed for the broadbeam data fit that produced the E_{crit} values for each of the shift register designs. After defining the proper critical energy value, the chosen environment is simulated thoroughly so that the underlying response distribution is properly (i.e., sufficiently) sampled. In this case, sampling the device response was straightforward since it is dominated by direct ionization and not energy deposited from secondary products resulting from ion-ion inelastic reactions. Direct ionization events account for the vast majority of ion-material interactions, so sampling the device response distribution does not require an inordinate amount of events.

Discussion

The present modeling approach, using a linear combination of weighted sensitive volumes to predict realistic device response, produces results that are consistent with experimental broadbeam testing and has been expanded to predict soft error rates in any well-defined environment, such as GCR. As mentioned earlier, this approach has already been validated for a CMOS SRAM structure [7], but it performs a very different function than the SiGe HBTs considered in this work.

The critical energy required for a soft upset is the key quantity needed for modeling phenomena within the MRED framework. This quantity subsumes all of the sensitivity information about the device and circuit into a single number. E_{crit} can then be used in other calculations to derive more complex quantities like cross sections and event rates. Using this methodology, once E_{crit} has been exceeded, an event must occur.

In an ideal situation, no additional scaling of the MRED output beyond the initial and logical factor of 127 would be necessary. However, it is difficult to determine exactly how many sensitive transistors are present in any given shift register stage at any one time during or immediately after an ion strike. At data rates above 1 Gbps, like those considered here, the transistors are switching at frequencies sufficient to sample many points of a single event transient current pulse. This means that the quasi-static approach of assuming that all the charge from a single event is integrated on a single sensitive node during one clock cycle is invalid. This conclusion is confirmed by the data presented in [10]. Despite this daunting complexity, the SEU cross section is saturated above 1 Gbps according to Fig. 11 of [3], meaning that the number of sensitive transistors is probably constant, though the types of soft errors may vary.

Beyond variable transistor sensitivity, it is critical to note what this calculation *is* and what it *is not*. The number calculated is not an error rate; it is an event rate. An error rate would imply some knowledge of the error length and error-internal bit patterns, like those outlined in [10]. The number calculated, however, is an event rate, meaning that at an energy of 2.7 MeV, there will be at most 1.2×10^{-5} events per day capable of depositing that much energy into the defined sensitive volume ensemble of a single transistor. The fact that this energy is the critical energy means that an event implies an error, though it implies nothing specific about the error. The error could be one, two, three, or many bits.

The model developed for the IBM 5AM SiGe HBT is also being applied to the IBM 7HP SiGe HBT. The data inputs include unpublished microbeam data as well as the broadbeam data in [2]. The rest of the modeling and the event rate calculation are analogous to the procedures explained herein. Since the IBM 7HP SiGe HBT is just a scaled version of the 5AM process [2], the current sensitive volume model will be scaled and validated. The sensitive volume model presented here could become a standard engineering tool for most SiGe HBT applications that use the IBM 5AM or 7HP SiGe HBT processes.

Conclusion

The modeling approach presented here represents a significant evolution in event rate calculations. This type of modeling is going to become increasingly critical as the circuits deployed into hostile radiation environments operate at higher speeds and rely on inherently complex geometries for operating characteristics and fabrication needs. This statement is not directed specifically at SiGe HBTs, though they are an excellent test bed for this approach due to their functional and geometric complexity as well as their unique radiation response.

References

[1] P. W. Marshall, M. A. Carts, A. Campbell, D. McMorrow, S. Buchner, R. Stewart, B. Randall, B. Gilbert, and R. A. Reed, "Single event effects in circuit-hardened SiGe HBT logic at gigabit per second data rates," *IEEE Trans. Nuc. Sci.*, vol. 47, no. 6, pp. 2669-2674, 2000.

[2] R. A. Reed, P. W. Marshall, J. C. Pickel, M. A. Carts, B. Fodness, G. F. Niu, K. Fritz, G. Vizkelethy, P. E. Dodd, T. Irwin, J. D. Cressler, R. Krithivasan, P. Riggs, J. Prairie, B. Randall, B. Gilbert, and K. A. LaBel, "Heavy-ion broad-beam and microprobe studies of single-event upsets in 0.20-mu m SiGe heterojunction bipolar transistors and circuits," *IEEE Trans. Nuc. Sci.*, vol. 50, no. 6, pp. 2184-2190, 2003.

[3] P. W. Marshall, M. Carts, S. M. Currie, R. A. Reed, B. Randall, K. Fritz, K. Kennedy, M. Berg, R. Krithivasan, and C. Siedleck, "Autonomous Bit Error Rate Testing at Multi-Gbit/s Rates Implemented in a 5AM SiGe Circuit for Radiation Effects Self Test (CREST)," *IEEE Trans. Nuc. Sci.*, vol. 52, no. 6, pp. 2446-2454, 2005.

[4] J. A. Pellish, R. A. Reed, R. D. Schrimpf, M. L. Alles, M. Varadharajaperumal, G. Niu, A. K. Sutton, R. Diestelhorst, G. Espinel, R. Krithivasan, J. P. Comeau, J. D. Cressler, G. Vizkelethy, P. W. Marshall, R. A. Weller, M. H. Mendenhall, and E. J. Montes, "Substrate engineering concepts to mitigate charge collection in deep trench isolation technologies," *IEEE Trans. Nuc. Sci.*, vol. 53, no. 6, pp. 3298-3305, 2006.

[5] E. J. Montes, R. A. Reed, J. A. Pellish, M. L. Alles, R. D. Schrimpf, R. A. Weller, M. Varadharajaperumal, G. Niu, A. K. Sutton, R. Diestelhorst, G. Espinel, R. Krithivasan, J. P. Comeau, J. D. Cressler, P. W. Marshall, and G. Vizkelethy, "Single event upset mechanisms for low energy deposition events in silicon germanium HBTs," *IEEE Trans. Nuc. Sci.*, to be published, 2007.

[6] D. E. Fulkerson, D. K. Nelson, and R. M. Carlson, "Boxes: an engineering methodology for calculating soft error rates in SOI integrated circuits," *IEEE Trans. Nuc. Sci.*, vol. 53, no. 6, pp. 3329-3335, 2006.

[7] K. M. Warren, B. D. Sierawski, R. A. Weller, R. A. Reed, M. H. Mendenhall, J. A. Pellish, and R. D. Schrimpf, "Predicting thermal neutron induced soft errors in static memories using TCAD and physics-based Monte-Carlo simulation tools," *IEEE Electron Device Lett.*, vol. 28, no. 2, pp. 180-182, 2007.

[8] R. A. Reed, R. A. Weller, R. D. Schrimpf, M. H. Mendenhall, K. M. Warren, and L. W. Massengill, "Implications of nuclear reactions for single event effects test methods and analysis," *IEEE Trans. Nuc. Sci.*, vol. 53, no. 6, pp. 3356-3362, 2006.

[9] A. J. Tylka, J. H. Adams Jr, P. R. Boberg, B. Brownstein, W. F. Dietrich, E. O. Flueckiger, E. L. Petersen, M. A. Shea, D. F. Smart, and E. C. Smith, "CREME96: a revision of the Cosmic Ray Effects on Micro-Electronics Code," *IEEE Trans. Nuc. Sci.*, vol. 44, no. 6, pp. 2150-2160, 1997.

[10] A. K. Sutton, R. Krithivasan, P. W. Marshall, M. A. Carts, C. Siedleck, R. Ladbury, J. D. Cressler, C. J. Marshall, S. Currie, R. A. Reed, G. Niu, B. Randall, K. Fritz, D. McMorrow, and B. Gilbert, "SEU error signature analysis of Gbit/s SiGe logic circuits using a pulsed laser microprobe," *IEEE Trans. Nuc. Sci.*, vol. 53, no. 6, pp. 3277-3284, 2006.

VI. SELs in TI CMOS (Vanderbilt University, NASA/GSFC, Texas Instruments)

Introduction

Single event latchup (SEL) has been a significant reliability concern for CMOS devices in radiation environments for the last twenty to thirty years [1-9]. As devices have scaled to smaller dimensions, with a concomitant decrease in the amount of deposited charge necessary to perturb voltages into a possible latching condition, there is the concern that circuits may become more susceptible to SEL [9-13]. In contrast to this potential trend toward increasing vulnerability, the scaling trend of electrical characteristics for new technology nodes works in the system designer's favor [14]. With reduction in the gain product of the two parasitic transistors involved in the latchup process and with the supply voltage scaling below the electrical holding voltage, latchup may be of less concern in future technologies. Here we analyze these competing trends in a 65nm technology using a combination of electrical measurements and 3-dimensional TCAD simulations. When considering the impact of scaling on SEL, one of the main considerations has been the anode-cathode spacing in the latchup structure. In this reseach we study the impact of scaling the width of transistors as well.

It should be noted that for reliability concerns, a simple test of the electrical holding voltages, gain products, and holding currents at room temperature may not be sufficiently robust to allay all concerns about latchup [15-17]. For a given application, the range of environment temperatures must be considered. We present results of our complete analysis of these parameters.

Device Structure

The device examined in this work is an NPNP structure from a test chip fabricated in a 65 nm CMOS technology. The layout is shown in figure 1a. The device was simulated and calibrated using measured electrical characteristics and doping profiles. The well contact is 10 µm from the anode and the substrate contact is 20 µm from the cathode. The anode and cathode represent the P-source and N-source in a CMOS structure, respectively. The N-well and the contacts for the N-well, P-anode, N-cathode, and P-substrate are 20 µm wide. Figure 1b shows the 3D TCAD device. To reduce computational time and memory constraints, the device is cut in half in TCAD to take advantage of the symmetrical properties of the structure. For all the biasing and temperature conditions in these simulations, the beta product of the two bipolar transistors is above unity. Therefore, holding voltage and holding current will be examined.

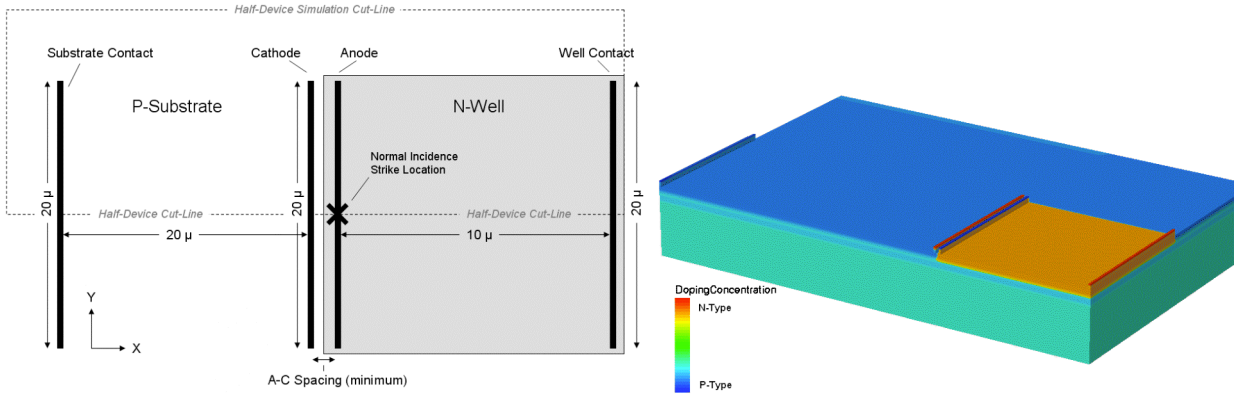


Figure 1: (a) Layout of physical SCR structure in 65nm technology with minimum anode-cathode spacing and maximum well and substrate contact spacing (b) TCAD structure for simulations. The "half" structure takes advantage of symmetry and reduces computational requirements.

Simulations and Results

Boselli et al. have shown that for the 65nm technology examined here, holding voltage exceeds the nominal operating voltage and room temperature [14]. However, modern commercial processors can operate within specifications up to almost 400 K and military spec requires devices to be tested up to 425 K. Figure 2 shows (a) the difference between holding voltage and operating voltage and (b) the holding current vs. device temperature for the simulated structure operated at nominal core voltage of 1.2 V.

It is important to understand how these electrical characteristics relate to the single event latchup vulnerability. Response from localized interactions at the junction inside the structure due to collected charge are potentially quite different than the electrical response created from voltages and currents seen at the terminals of the structure. Initial SEL simulations were carried out using an LET of 80 MeV-cm^2-mg^{-1}, normal incidence to the surface on the edge of the simulated region (corresponding to the middle of the physical device) and directly through the anode contact. All simulated ion track lengths are 20 μ long. It was previously shown that the portion of the N-well farthest away from the well contact is the most sensitive region of the structure for initiating latch-up [6, 7]. The simulations were performed at nominal voltage for the technology (1.2 V) with varying temperature. The results are shown in figure 3.

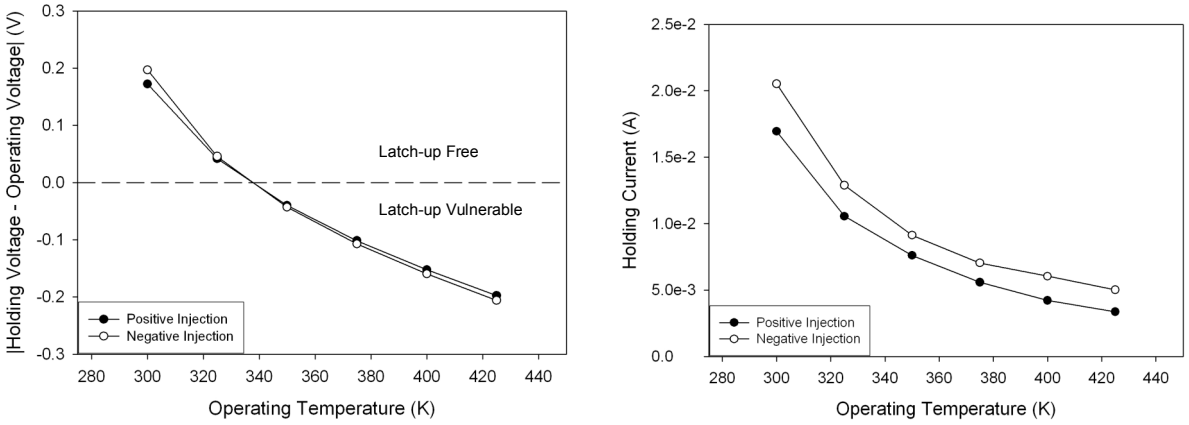


Figure 2: Latchup vulnerability for 65 nm NPNP device with minimum A-C spacing. (a) Difference in holding voltage and operating voltage vs. temperature. The plot is divided into "latch-up free" and "latch-up vulnerable" regions. (b) Holding current vs. operating voltage.

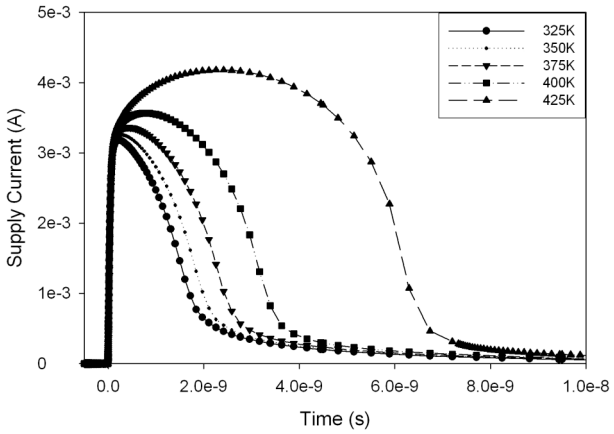


Figure 3: Single event response current vs. time for varying temperatures at nominal operating voltage (1.2 V). The current at the tied anode/Nwell contacts is plotted

Figure 3 shows that the structure does not latch up for 80 MeV-cm^2-mg^{-1} normal incidence strikes. At first glance, this could be assumed to be because the device currents are below the holding currents for their respective operating conditions. The very long pulse seen in the 425K test at nominal (1.2 V) operating voltage is an example of the structure "almost" latching. However, examination of the plotted potentials for that event shows that about two-thirds of the width of the structure (closest to the strike) reaches a potential sufficient to cause latchup. Figure 4 shows the potential in the N-well referenced from the N-well contact 2.0 ns after the 80 MeV-cm^2-mg^{-1} particle strike. It can be seen that even for this very high LET strike, the structure does not fully latch along the entire junction and can recover. The regenerative feedback in the

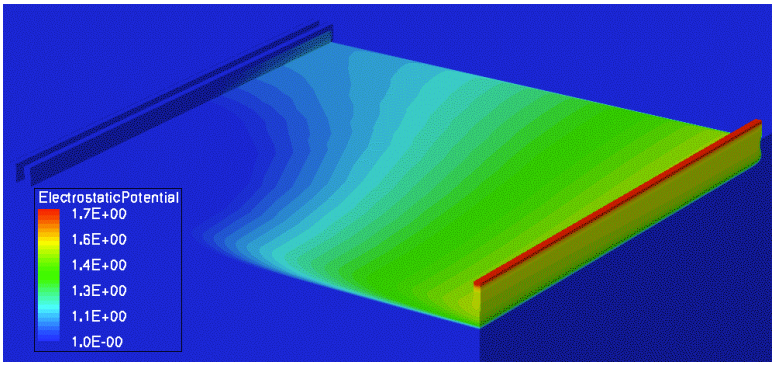


Figure 4: (a) Potential plot for 425K temperature pulse seen in figure 3b at t = 2.0 ns. In dark red is the potential of the N-well contact. Dark blue is a 0.7 V potential difference (diode drop) from that contact. About 6 µm (out of 10 µm) of the width of the device have the proper biasing for latchup.

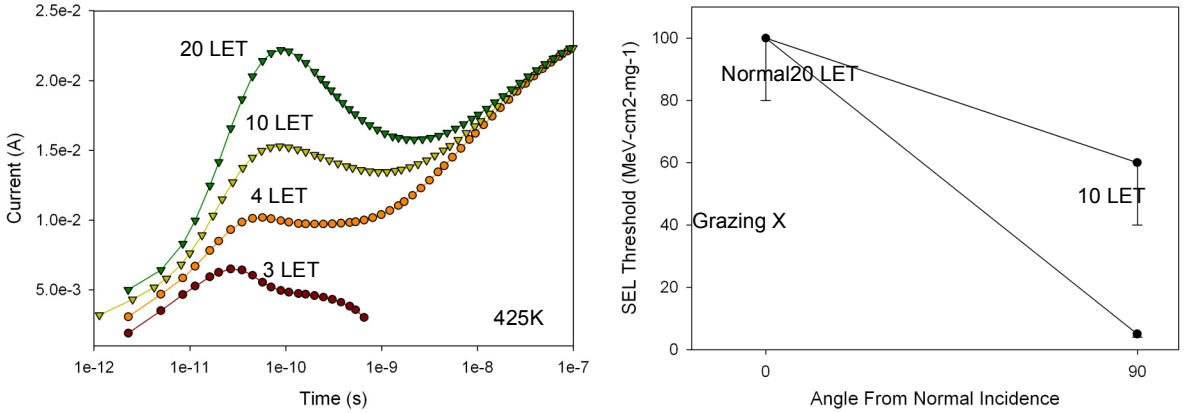


Figure 5: (a) Single event response current vs. time for varying temperatures at nominal operating voltage (1.2 V) and 425K for varying LET at grazing angle parallel to the anode. The current at the tied anode/Nwell contacts is plotted (b) Threshold for SEL at normal incidence and grazing angles in both the x and y directions for 425K operation

regions of the structure where the device is latched contributes to the long pulse seen in figure 3. Normal incidence strikes at 100 MeV-cm^2-mg^{-1} were sufficient to latch the structure.

To further investigate the vulnerability of the structure, an extreme grazing angle test simulation was performed. For these tests, an ion strike parallel to the surface (Y direction in figure 1a) was placed directly under the anode across the entire N-well width. These simulations were run at 425K and nominal (1.2 V) voltage. As can be seen in figure 5a, a particle of much lower energy is sufficient to latch the device with this strike orientation. The threshold is somewhere between 3 and 4 MeV-cm^2-mg^{-1}. The 3 MeV-cm^2-mg^{-1} strike does not latch the structure since it does not achieve the holding current required in figure 2b. Strikes at a grazing angle in the X direction were also tested and placed in the center of the N-well in the test structure (along the half device cut line in figure 1a) coming from the device boundary on the N-well side. Figure 5a shows the change in threshold LET between normal incidence to the surface and grazing strikes at right angles to each other. It can be seen that the device is much more sensitive to a grazing angle strike that occurs parallel to the N-well/Substrate boundary underneath the anode than to a grazing angle strike perpendicular to the anode contact. This angular effect can be explained in two ways. The first of these is the conventional "sensitive volume". With a long (narrow and shallow) sensitive volume underneath the length of the anode with the distance from the STI to the N-well/Substrate boundary as the vertical dimension, even a low LET strike of 4 MeV-cm^2-mg^{-1} at a grazing angle will deposit more energy over the 10µm width than a normal incidence strike with an LET of 80 MeV-cm^2-mg^{-1}. The same could be said for the grazing angle strike in the X direction. With a sensitive volume defined only near the anode, most of the charge would be deposited in

the N-well outside of the sensitive volume. The second explanation is that latching is a localized phenomenon in devices. While a large 80 MeV-cm^2-mg^{-1} strike can deposit a significant amount of charge even in a shallow N-well, it only latches the PNPN structure within several microns of the strike. Not only does it matter how much energy is deposited in a sensitive volume, the spatial distribution of that energy is critical in determining whether latchup occurs. Although this is a more extreme aspect ratio than seen in other studies due to the large size of the test structure, the results seen in figure 5b are consistent with work by other researchers that shows large increases in latchup cross section with temperature and angle [4, 15, 18]. In [15], significant increases in cross section at grazing angle are seen at proton energies where the reaction products are forward directed. In this case reaction products with lower LETs do not latch the SRAMs until oriented along the N-well/Substrate boundaries near P-source contacts. Therefore, for predictive TCAD simulations it will be absolutely crucial to understand the physical processes and statistical distribution of proton fragmentation products at varying energies. Due to the large aspect ratio of the sensitive volume in these structures, the change in SEL threshold is much more pronounced with angle than the results seen in [15] but the trend is the same. This leads to the conclusion that the magnitude of the change in SEL threshold with angle is directly related to the width of the devices. In addition to this observation, figure 5b suggests it is possible that an extra axis is needed to properly characterize the effects of angle. Simply tilting the device under test to grazing angle will orient ions and forward directed secondary particles either parallel or normal to the longest component of the individual sensitive volumes in an SRAM. Once at grazing angles, rotating the test fixtures laterally will likely result in an observable change in threshold and cross section. For most deep submicron technologies, a test will also need to be performed with the die above room temperature (observing a chart like figure 2a) in order to see latchup.

Conclusions

We have demonstrated here both the effects of temperature and angle in determining the vulnerability of PNPN structures to SEL. Due to the large aspect ratio of the simulated structure, a significant change in threshold LET was observed with variable angle of incidence for simulated heavy ion strikes. It is suggested that researchers should examine the effects of angle using two axes in tests as particles not moving parallel to the edges of the N-well near P-sources are less likely to instigate latching. Using techniques such as the ones seen here, a predictive technique for sensitivity with angle should be able to be developed given a specific cell layout. Microbeam testing of these devices will be undertaken to better understand the simulation work seen here.

References

[1] K. Kinoshita, et al., "Radiation induced regeneration through the P-N junction in monolithic IC's," *IEEE TNS*, vol. 12, pp. 83-90, 1965.

[2] K. Soliman et al., "Latchup in CMOS from heavy ions," *IEEE TNS*, vol. 30, pp. 4514-4519, 1983.

[3] W. A. Kolasinski et al., "Simulation of cosmic-ray induced soft errors and latchup in integrated-circuit computer memories," *IEEE TNS*, vol. 26, pp. 5087-5091, 1979.

[4] L. Adams et al., "A verified proton-induced latchup in space," *IEEE TNS*, vol. 39, pp. 1804-1808, 1992.

[5] D. K. Nichols et al., "An observation of proton-induced latchup," *IEEE TNS*, vol. 39, pp. 1654-1656, 1992.

[6] A. H. Johnston et al., "Latchup in integrated circuits from energetic protons," *IEEE TNS*, vol. 44, pp. 2367-2377, 1997.

[7] A. H. Johnston, "The influence of VSLI technology on radiation-induced latchup in space systems," *IEEE TNS*, vol. 43, pp. 505-521, 1996.

[8] P. E. Dodd et al., "Neutron-induced soft errors, latchup, and comparison of SER test methods for SRAM technologies," IEDM, 2002.

[9] P. E. Dodd et al., "Neutron-induced latchup in SRAMs at ground level," IRPS, 2003.

[10] R. Baumann, "Single-Event Effects in Advanced CMOS Technology," NSREC Short Course, 2005.

[11] D. McMorrow et al., "Laser-induced latchup screening and mitigation in CMOS devices," *IEEE TNS*, vol. 53, pp. 1819-2006, 2006.

[12] J. R. Schwank et al., "Effects of particle energy on proton-induced single-event latchup," *IEEE TNS*, vol. 52, pp. 2622-2629, 2005.

[13] W. Morris, "Latchup in CMOS," IRPS, 2003.

[14] G. Boselli et al., "Latch-up in 65nm CMOS technology: a scaling perspective," IRPS, 2005.

[15] J. R. Schwank et al., "Effects of angle of incidence on proton and neutron-induced dingle-event latchup," *IEEE TNS*, vol. 53, pp. 3122-3131, 2006.

[16] A. H. Johnston et al., "The effect of temperature on single-particle latchup," *IEEE TNS*, vol. 38, pp. 1435-1441, 1991.

[17] W. A. Kolasinski et al., "The effect of elevated temperature on latchup and bit errors in CMOS devices," *IEEE TNS*, vol. 33, pp. 1605-1609, 1986.

[18] P. J. McNulty et al., "Simple model for proton-induced latch-up," *IEEE TNS*, vol. 40, pp. 1947-1951, 1993.

VII. MBUs in TI CMOS (Vanderbilt University, NASA/GSFC, Texas Instruments)

Introduction

Multiple-bit upset (MBU) has increased in recent complementary metal-oxide-semiconductor (CMOS) technology generations [1]. For static random access memory (SRAM), integrated circuit scaling has decreased the distance between sensitive volumes making MBU more likely. This is not the case for single event upset (SEU) cross section. The varied trends among sensitive volume size, voltage supply, and charge sharing have generally held the SEU cross section constant across process generations [2]. The increasing problem of MBU must be considered in the context of memory architecture, layout, and design for state-of-the-art and future technology nodes.
In this work we examine neutron-induced MBU in an SRAM for a 90 nm CMOS technology. Experimental neutron irradiation shows increased MBU probability for neutrons incident at grazing angles. The physical mechanisms for MBU are examined using the MRED (Monte Carlo Radiative Energy Deposition) code and the results are compared to experimental data.

Experimental

Neutron irradiations of a 90 nm CMOS SRAM were carried out at Los Alamos National Laboratory's Weapons Neutron Research (WNR) facility. The device under test was a high performance 1.2 V 6T SRAM with cell dimensions of 1.47 μm x 0.66 μm (0.97 μm^2). The memory was periodically read to record bit-errors. Error data were time-stamped so that MBUs could be identified. In this experiment MBU was defined as two or more physically adjacent bits failing with the same time stamp and counted as one MBU event.

The neutron-induced SEU cross section is plotted versus angle in Fig. 1. The experimental SEU cross section varies little with angle of incidence. The simulation results indicated by red squares are discussed in Section **Error! Reference source not found.**. The probability of MBU is defined as the ratio of the number of MBU events to the number of total SEU events and is shown in Fig. 2. The probability that an event induces MBU increases for angles farther from normal incidence.

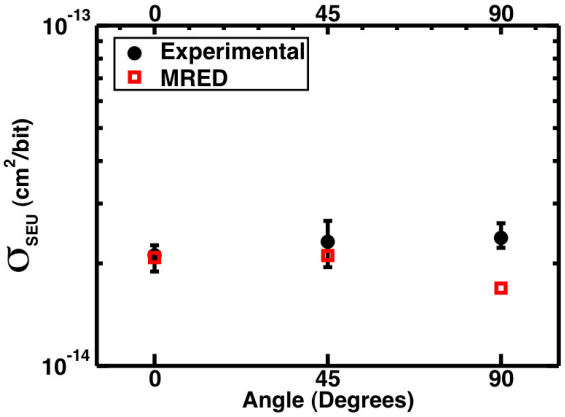


Fig. 1. Experimental SEU cross section from neutron irradiation. The SEU cross section is constant with respect to angle of irradiation. The simulated SEU cross section from MRED is indicated by red squares.

Discussion

CMOS transistor test structures were fabricated in the same 90 nm process to determine the charge collection depth. Ion beam induced charge collection (IBICC) was performed on these devices at Sandia National Laboratory as in [3]. The devices were irradiated using normally incident 36 MeV oxygen ions. The xy-position and total collected charge were recorded for each ion. The charge collection depth was estimated using the maximum collected charge of 60 fC as a worst case estimate as in [4]. The linear energy transfer (LET) of 36 MeV oxygen is 6 MeV-cm^2/mg or 60 fC/μm. The charge collection depth for this process is estimated to be 1 μm.

Energy deposition simulation for the device under test were calculated using MRED. MRED is a Monte-Carlo transport code based on Geant4 [5, 6]. A 3-dimensional technology computer aided design (TCAD) structure was created from the SRAM layout and process information of the device under test.

The TCAD structure was imported into MRED and neutron irradiation was carried out using the WNR beam flux spectrum. Neutron transport through the TCAD structure was simulated in MRED. The recorded energy deposition for each neutron event and the overall energy deposition cross section were calculated based on the methods described in [4]. Corresponding sensitive volumes for an array of 420 SRAM cells were placed in the structure. The dimensions of each sensitive volume were 0.45 μm x 0.45 μm x 1.0 μm, based on the drain area of an off-state NMOS transistor.

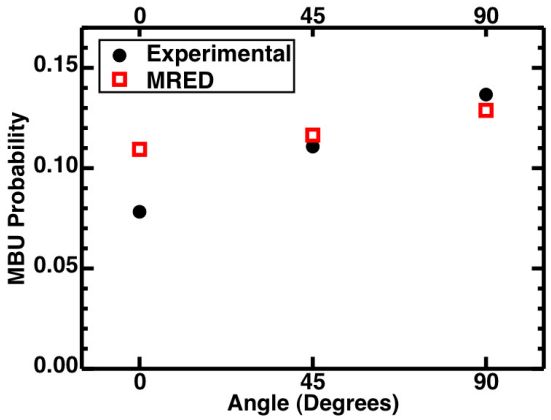


Fig. 2. The MBU probability as a function of angle. Grazing angles show an increased probability. The simulated MBU probabilities from MRED are indicated by red squares.

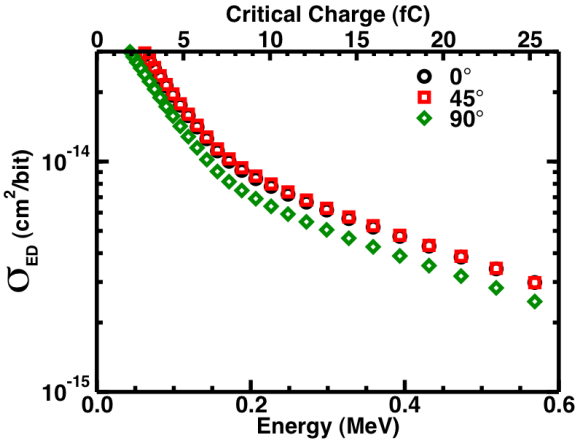


Fig. 3. The MRED single volume energy deposition cross section σ_{ED} from neutron irradiation.

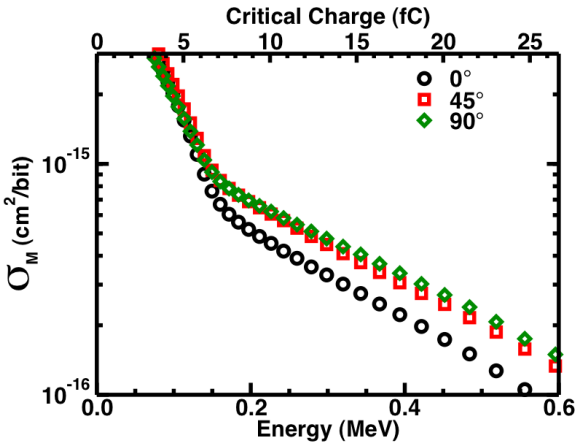


Fig. 4. The MRED multiple volume energy deposition cross section σ_M from neutron irradiation. The structure exhibits little change in cross section with respect to angle.

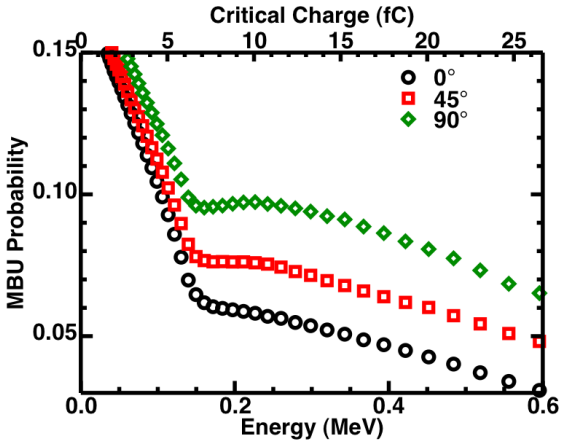


Fig. 5. The MRED probability of MBU. The probability of MBU nearly doubles for neutrons at grazing angles.

Results

The single volume energy deposition cross section σ_{ED} and multiple volume energy deposition cross section σ_M are shown in Fig. 3 and Fig. 4 respectively. The σ_{ED} exhibits a small decrease at grazing angles while σ_M increases with increasing angle of incidence.

The probability of MBU is shown in Fig. 5. The probability increases for neutrons at grazing angles. Critical charge Q_{CRIT} is the amount of charge required to induce upset. Spectre circuit simulations of the tested SRAM cell show a critical charge of approximately 4 fC. For this value of Q_{CRIT}, Fig. 1 shows the correlated σ_{SEU} from the MRED calculated σ_{ED} and Fig. 2 shows the correlated MBU probability from the MRED calculated σ_{ED} and σ_M. Simulation data are in good agreement with the experimental data for Q_{CRIT} of 4 fC.

The simulated MBU probabilities in Fig. 5 show the same trends as the experimental data in Fig. 1. As the angle of incidence increases, so does the probability of MBU events. The probability of MBU events nearly doubles for neutron irradiation at large angels of incidence. The experimental and simulated probabilities for the WNR neutron beam exhibit MBU probability from 8-14%. The MBU probability nearly doubles at grazing angles for higher Q_{CRIT}.

Conclusion

Neutron irradiation has been performed on a 90 nm CMOS SRAM. Experimental data and MRED simulation show that the SEU cross section varies little with angle of incidence, but the probability of MBU increases at grazing angles. Simulation of these data using MRED are in good agreement with the experimental data.

References

[1] N. Seifert, P. Slankard, M. Kirsch, B. Narasimham, V. Zia, C. Brookreson, A. Vo, S. Mitra, B. Gill, and J. Maiz, "Radiation-Induced Soft Error Rates of Advanced CMOS Bulk Devices," pp. 217 - 225, 2006.

[2] R. C. Baumann, "Radiation-induced soft errors in advanced semiconductor technologies," *IEEE Transactions on Device and Materials Reliability*, vol. 5, no. 3, pp. 305-316, SEP 2005.

[3] R. A. Reed, P. W. Marshall, J. C. Pickel, M. A. Carts, B. Fodness, G. F. Niu, K. Fritz, G. Vizkelethy, P. E. Dodd, T. Irwin, J. D. Cressler, R. Krithivasan, P. Riggs, J. Prairie, B. Randall, B. Gilbert, and K. A. LaBel, "Heavy-ion broad-beam and microprobe studies of single-event upsets in 0.20-mu m SiGe heterojunction bipolar transistors and circuits," *IEEE Transactions on Nuclear Science*, vol. 50, no. 6, pp. 2184-2190, DEC 2003.

[4] A. D. Tipton, J. A. Pellish, R. A. Reed, R. D. Schrimpf, R. A. Weller, M. H. Mendenhall, B. Sierawski, A. K. Sutton, R. M. Diestelhorst, G. Espinel, J. D. Cressler, P. W. Marshall, and G. Vizkelethy, "Multiple-Bit Upset in 130 nm CMOS Technology," vol. 53, no. 6, pp. 3259 - 3264, DEC 2006.

[5] S. Agostinelli, J. Allison, K. Amako, J. Apostolakis, H. Araujo, P. Arce, M. Asai, D. Axen, et al., "Geant4-a Simulation Toolkit," *Nuclear Instruments & Methods in Physics Research Section a-Accelerators Spectrometers Detectors and Associated Equipment*, vol. 506, no. 3, pp. 250-303, JUL 1 2003.

[6] M. H. Mendenhall and R. A. Weller, "An algorithm for computing screened Coulomb scattering in GEANT4," *Nuclear Instruments & Methods in Physics Research Section B-Beam Interactions with Materials and Atoms*, vol. 227, no. 3, pp. 420-430, JAN 2005.